

Geology

May 2017, Volume 45 Issue 5 Pages 471-474

<https://doi.org/10.1130/G38778.1><https://archimer.ifremer.fr/doc/00773/88502/>**Archimer**<https://archimer.ifremer.fr>

Origin of the dunitic mantle-crust transition zone in the Oman ophiolite: The interplay between percolating magmas and high-temperature hydrous fluids

Rospabé Mathieu ¹, Ceuleneer Georges ¹, Benoit Mathieu ¹, Abily Bénédicte ¹, Pinet Patrick ²¹ Univ Toulouse, CNRS, IRD, GET, Observ Midi Pyrenees, 14 Ave E Belin, F-31400 Toulouse, France.² Univ Toulouse, CNRS, IRD, IRAP, Observ Midi Pyrenees, 14 Ave E Belin, F-31400 Toulouse, France.

Abstract :

Determining which petrological processes build the mantle-crust dunitic transition zone (DTZ) in oceanic spreading settings has a direct impact on our understanding of thermal and chemical transfers on Earth. We report on understated but widespread mineral assemblages present in the DTZ at the top of a mantle diapir (Oman ophiolite), including pargasite, grossular, and pyroxenes of peculiar composition. These minerals are present interstitially between olivines and as inclusions in the disseminated chromite grains, indicating that they are early, high-temperature features. They call for hybridization between the mid-oceanic ridge basalt melts that fed the crustal section and supercritical water saturated with silica. Our synoptic survey (similar to 300 samples collected along 11 cross sections) demonstrates that the DTZ was pervasively infiltrated by such hybrid melts and that the abundance of their crystallization products increases upsection, likely in response to increasing supply of water and decreasing temperature. This indicates that water is involved in the reaction leading to the transformation of mantle harzburgite into dunite in the DTZ. On the basis of field evidence, a hydrothermal origin of the water is a reasonable hypothesis.

27 INTRODUCTION

28 In ophiolites, and especially in Oman, the contact between the mantle peridotites
29 and the lower crust is underlined by a horizon as much as several hundred meters thick
30 made essentially of dunite (>95% olivine + minor chromite). The origin of this dunitic
31 transition zone (DTZ) was questioned in the pioneering studies of Moores and Vine
32 (1971) and Greenbaum (1972) and is still debated. The DTZ has been viewed as the
33 shallowest part of the mantle, i.e., a residue of reaction melting between host harzburgite
34 and a percolating melt becoming undersaturated in silica relative to orthopyroxene (Opx)
35 at low pressure (e.g., Moores and Vine, 1971; Dick, 1977; Rabinowicz et al., 1987), or as
36 the deepest part of the crust, i.e., cumulates from Mg-rich melts (e.g., Greenbaum, 1972;
37 Elthon, 1979). We have shown that the two options are not mutually exclusive and that
38 the DTZ can include both residual and cumulative horizons (Abily and Ceuleneer, 2013).

39 We have performed a systematic sampling of the DTZ in the Maqsad area and,
40 based on our sampling collection (>300 sampling sites), we realized that the DTZ
41 exposes an unexpected abundance of discreet mineral assemblages of enigmatic origin
42 (partly igneous, partly hydrous). The distribution of these mineral assemblages is not
43 random, but vertical within the DTZ. We propose that they are a clue to understand the
44 petrological processes involved in the formation of the DTZ.

45 GEOLOGICAL SETTING AND FIELD OCCURENCE

46 The upper Cretaceous Oman ophiolite issued from the Tethys Ocean.
47 It is made of two contrasting magma series: one is a mid-oceanic ridge basalt (MORB)
48 type and the other has a depleted andesitic affinity attributed to subduction and/or
49 thrusting or to hydrated remelting of the shallow lithosphere during spreading (e.g.,
50 Pearce et al., 1981; Benoit et al., 1999; Python and Ceuleneer, 2003; Yamasaki et al.,
51 2006; MacLeod et al., 2013).

52 The Maqsad area (Sumail massif), the focus of our study (Fig. 1), exposes a
53 former asthenospheric diapir that contributed a large amount of melt into the crust
54 (Rabinowicz et al., 1987). It fed a ridge segment extending to the northwest and southeast
55 of the diapir for a distance of ~80 km (Python and Ceuleneer, 2003). It evolved in a
56 MORB igneous environment (Ceuleneer et al., 1996; Benoit et al., 1996; Korenaga and
57 Kelemen, 1997).

58 A few faults parallel to the paleo-ridge direction (northwest-southeast) affect the
59 DTZ. They consist of breccia with serpentine and carbonate matrix, frequently intruded
60 by gabbroic dikes altered in greenschist facies conditions. They are zones of intense fluid
61 circulation that underwent moderate normal fault movement. Away from them, dunite is
62 weakly serpentized (<20%); this has preserved its high-temperature mineral
63 assemblages. Above the Maqsad diapir the DTZ was not transposed off axis by mantle
64 corner flow, and the massif as a whole was not affected by late tectonic events (Ceuleneer
65 et al., 1988).

66 **PETROLOGY AND MINERAL CHEMISTRY**

67 We sampled the Maqsad DTZ with a vertical step of 10–20 m along 12 cross
68 sections extending from the mantle harzburgites to the layered cumulates (Fig. 1C). All

69 samples (~300) as well as ~400 silicate inclusions enclosed in chromite grains were
70 analyzed with the electron microprobe.

71 The Maqсад DTZ, 200–350 m thick, is made of alternating metric to decametric
72 horizons of pure dunites and dunites containing variable amounts of interstitial
73 clinopyroxene (Cpx) and plagioclase (Fig. 2). The abundance of these interstitial
74 minerals, witnesses of melt percolation, and the degree of differentiation increase upward
75 in most sections, e.g., lower Mg# ($100 \times \text{Mg}/[\text{Mg} + \text{Fe}_{\text{Total}}]$) in olivine and Cpx, lower
76 NiO in olivine, and higher TiO₂ in chromite.

77 In addition to large (millimeter to centimeter) interstitial and poikilitic Cpx
78 compositions (Cr, Al, and Ti rich) consistent with an igneous origin, tiny (tens to
79 hundreds of microns) Cpx crystals underline olivine grain rims (Fig. 3A).
80 They display high Mg# ($93 < \text{Mg\#} < 99$) and CaO (>25 wt%) and low Al₂O₃, Cr₂O₃, and
81 TiO₂ contents (see the GSA Data Repository¹). These compositions are spread between
82 two end members, the igneous Cpx and the diopsides found in hydrothermal diopsidite
83 veins (Python et al., 2011) (Fig. 4A). They are observed in two-thirds of the samples,
84 distributed across the DTZ and particularly abundant at the top of the diapir. Inclusions of
85 Cpx in chromite exhibit the same range of compositions.

86 Among the other **exotic** [[SU: should not be in quotes. “exotic” has specific
87 **geological meaning (i.e., foreign or introduced); is meaning here “unusual” or**
88 **similar?]] interstitial phases, we observed grossular garnet (37 samples; Fig. 3B),
89 amphibole (pargasites and magnesio-hornblendes) (41 samples; Fig. 3C), and enstatite
90 (Opx, 19 samples; Fig. 3D). Almost all occurrences of amphibole and garnet are in the
91 upper half of the DTZ (>~150 m above its base), and Opx is restricted to its upper part**

92 (>~250 m) (Fig. 2). The vertical distribution of each mineral phase in inclusions in
93 chromite grains perfectly mimics their distribution in the olivine matrix.

94 Interstitial calcic amphiboles (Fig. 3C) have a lower TiO₂ content (mostly <0.2
95 wt%) than those in inclusions in chromite (0.2–0.9 wt%) (Fig. 4B). This can be attributed
96 to chemical exchange with the host chromites. All amphiboles (both interstitial and
97 enclosed in chromite) display a common evolution of (Na⁺K)_A element concentration
98 from 0.4 to 1. DTZ Opx forms oikocrysts with lobate contacts with olivine, in obvious
99 contrast to their porphyroclastic texture in mantle harzburgite (Fig. 3D). The composition
100 of the two kinds of Opx is also contrasted (Fig. 4C): DTZ Opx (both oikocrysts and
101 inclusions in chromite) have a much higher TiO₂ content for similar Mg#, reaching 0.37
102 wt% (average = 0.2 wt%). Among the ~400 analyzed inclusions in chromite (Figs. 3E,
103 3F), 40% = amphibole (mostly pargasite), 39% = igneous Cpx, 7% = hybrid diopside, 7%
104 = olivine, 3% = mica (Na-rich aspidolite and K-rich phlogopite), 3% = Opx, and 1% =
105 plagioclase and garnet.

106 INVOLVMENT OF A HYDROUS MELT IN THE GENESIS OF THE DTZ

107 Variations in the distribution of the interstitial minerals evoke crystallization from
108 a percolating melt in response to compaction (Rabinowicz et al., 1987). In previous
109 studies, the origin of the DTZ has been discussed in a dry igneous system. Interstitial,
110 igneous, Ti-rich Cpx indicates that a MORB melt percolated through the Maqsad DTZ
111 (Abily and Ceuleneer, 2013; this study). This is also evidenced by the composition of the
112 feeding melt channels entrapped in the underlying mantle harzburgite (Kelemen et al.,
113 1995; Ceuleneer et al., 1996; Benoit et al., 1996) and by the composition of the
114 troctolitic-gabbroic sills inside the DTZ (Korenaga and Kelemen, 1997). However, the

115 nature and abundance of the **exotic** minerals call for pervasive percolation of another
116 water- and silica-rich melt throughout the DTZ that occurred early, as demonstrated by
117 the entrapment of these minerals in the chromite grains. This leads us to formulate the
118 hypothesis that the hydrous melt percolation did not occur after dunite formation, but that
119 it contributed to the process that built the DTZ.

120 The possibility of a hydrous origin of dunites at a temperature significantly lower
121 than the liquidus of dry basaltic melts was stressed in the seminal work of Bowen and
122 Tuttle (1949). Addition of water to the system triggers the incongruent melting of
123 enstatite into olivine and silica melt. Dunite will form, and excess silica produced by this
124 reaction is exported from the system. Opx will eventually crystallize where this silica-
125 enriched melt accumulates and cools. The absence of Opx in the lower part of the DTZ
126 and its crystallization at its top is elegantly accounted for in this frame.

127 **ORIGIN OF WATER**

128 A water-saturated melt can have different origins: (1) a mantle source hydrated in
129 a subduction setting (e.g., MacLeod et al., 2013), (2) a shallow lithospheric source
130 hydrated by hydrothermal fluids and undergoing remelting in response to the rise of a
131 mantle diapir (Benoit et al., 1999), (3) an extreme degree of fractional crystallization of a
132 dry (actually water poor) MORB, and (4) hybridization of a MORB with hydrothermal
133 fluids.

134 In the first two hypotheses, the mantle source is depleted in incompatible
135 elements, including Ti. Primitive cumulates rich in Opx are widespread in the ophiolite
136 but crystallized from highly depleted melts (Benoit et al., 1999; Python and Ceuleneer,
137 2003; Akizawa and Arai, 2009). High Mg# in interstitial Opx in dunite seems **to**

138 contradict MORB involvement (e.g., Wang et al., 2016) but not the high Ti content.
139 Moreover, the successive occurrences of garnet, amphibole, and then Opx upsection (Fig.
140 2) are not in accordance with a deep-water source, which should have delivered hydrated
141 melt across the DTZ. The third hypothesis is difficult to reconcile with the high Mg# of
142 Opx and the abundance of amphibole: even if we consider that the Mg# is partly buffered
143 by high-forsterite olivine, the degree of fractional crystallization necessary to reach water
144 saturation should be far too high (Gillis and Meyer, 2001).

145 This led us to explore the fourth hypothesis. The percolation of high-temperature
146 hydrothermal fluids in the Oman lower oceanic crust is well documented (e.g., Coogan,
147 2003; Bosch et al., 2004; Akizawa et al., 2011; Koepke et al., 2014). The distribution of
148 hydrous minerals in the DTZ is consistent with the involvement of hydrothermal water.
149 The fact that Cpx composition spreads between igneous and hydrothermal end members
150 (Fig. 4A) is strong evidence for hybridization. We propose that the hybrid melt is a blend
151 between supercritical hydrothermal fluids rich in silica, i.e., trondhjemitic melt issued
152 from hydrous melting of the country rocks (Amri et al., 1996), and variably evolved
153 MORB.

154 Synmagmatic faults are present at the base of the Maqsad lower crust and were
155 main avenues for seawater penetration down to the Moho (Abily et al., 2011). The brittle
156 features affecting the DTZ may be the late expressions of faults that were active earlier.
157 They mainly affect the top of the DTZ and are, with the hydrous mineral distribution
158 (Fig. 2), consistent with a water supply from above. The presence of Opx and amphibole
159 in layered gabbroic cumulates in present-day oceanic lower crust was also explained by
160 the involvement of hydrothermal fluids (Gillis and Meyer, 2001) and by the extraction

161 from the mantle of heterogeneous batches of slightly evolved and unmixed melt (Gillis et
162 al., 2014).

163 **THERMAL AND CHEMICAL GEODYNAMIC IMPLICATIONS**

164 Interstitial hydrous minerals described in this study crystallized early, as shown
165 by similar phases enclosed in chromite grains. Purely hydrothermal alteration followed
166 the magmatic activity, as indicated by Cpx and amphibole alteration products (Fig. 4B)
167 and the presence of hydrogrossular and serpentine (see also Gregory and Taylor, 1981),
168 but obviously did not totally overprint the high-temperature features. This suggests a high
169 cooling rate of the DTZ, consistent with previous geothermometric studies of the base of
170 the Oman lower crust (VanTongeren et al., 2008) and uppermost mantle section (Dygart
171 and Liang, 2015).

172 Below a 5–6-km-thick crust, the stability field for Opx and amphibole after
173 fractionation from a primitive (virtually dry) to a highly evolved (water-saturated)
174 MORB may imply temperature decrease to ~950 °C (pressure of 0.2 GPa) (Berndt et al.,
175 2005). High-temperature conditions of crystallization of diopside from hybrid melts are
176 supported both by their entrapment in chromite and their coexistence with igneous Cpx.
177 Regarding the composition range pointing toward igneous Cpx, the crystallization
178 temperature of diopside seems to be higher than the 600–800 °C previously estimated for
179 a pure hydrothermal frame (Python et al., 2007; Arai and Akizawa, 2014). Although the
180 garnet stability field is variable (300–800 °C) (e.g., Bach and Klein, 2009; Newton and
181 Manning, 2007), inclusions of andradite and grossular in chromites show that they also
182 fractionated at a high temperature. Considering that a dry MORB injected at Moho level
183 during the rise of the Maqsad diapir reached 1230 °C (Ceuleneer et al., 1996), the

184 mineralogical distribution through the DTZ (Fig. 2) points toward a thermal gradient of
185 about few hundreds degrees in only few hundred meters, making the Moho a clear
186 rheological transition between the hot ductile mantle above the diapir and the lower crust.

187 **CONCLUSIONS**

188 We propose that the formation of the DTZ bears witness to transient processes
189 attributable to the meeting, at Moho level, of an ascending front of mantle partial melts
190 and a descending front of hydrothermal fluids. This specific context triggers the
191 formation of hybrid melts out of equilibrium with their country rocks, which contribute to
192 deeply modify the mineralogical and geochemical composition of the shallow mantle and
193 deep crust. Furthermore, hydrous melts are well known to be particularly efficient in
194 mobilizing metals, such as Cr, in the formation of chromitite ore bodies (Borisova et al.,
195 2012). Our results suggest that the DTZ is among the most reactive interfaces on Earth.
196 Its formation may be a major factor in the global chemical transfer and redistribution
197 between the mantle, the crust, and the ocean, and can condition the cycle of carbon,
198 halogens, and gases such as hydrogen and methane.

199 Our views, although challenging, do not fully contradict previous models for the
200 genesis of the DTZ, but reconcile different pieces of evidence in a more general scenario.

201 **ACKNOWLEDGMENTS**

202 We thank S. Gouy, J. Langlade, and P. de Parseval for help in microprobe data
203 acquisition. Financial support was provided by the Centre National de la Recherche
204 Scientifique–Institut National des Sciences de l'Univers. Constructive reviews by N.
205 Dygert and N. Akizawa helped to improve our paper.

206 **REFERENCES CITED**

- 207 Abily, B., and Ceuleneer, G., 2013, The dunitic mantle-crust transition zone in the Oman
208 ophiolite: Residue of melt-rock interaction, cumulates from high-MgO melts, or
209 both?: *Geology*, v. 41, p. 67–70, doi:10.1130/G33351.1.
- 210 Abily, B., Ceuleneer, G., and Launeau, P., 2011, Synmagmatic normal faulting in the
211 lower oceanic crust: Evidence from the Oman ophiolite: *Geology*, v. 39, p. 391–394,
212 doi:10.1130/G31652.1.
- 213 Akizawa, N., and Arai, S., 2009, Petrologic profile of peridotite layers under a possible
214 Moho in the northern Oman ophiolite: An example from Wadi Fizh: *Journal of*
215 *Mineralogical and Petrological Sciences*, v. 104, p. 389–394,
216 doi:10.2465/jmps.090622a.
- 217 Akizawa, N., Arai, S., Tamura, A., Uesugi, J., and Python, M., 2011, Crustal diopsidites
218 from the northern Oman ophiolite: Evidence for hydrothermal circulation through
219 suboceanic Moho: *Journal of Mineralogical and Petrological Sciences*, v. 106,
220 p. 261–266, doi:10.2465/jmps.110621b.
- 221 Amri, I., Benoit, M., and Ceuleneer, G., 1996, Tectonic setting for the genesis of oceanic
222 plagiogranites: Evidence from a paleo-spreading structure in the Oman ophiolite:
223 *Earth and Planetary Science Letters*, v. 139, p. 177–194, doi:10.1016/0012-
224 821X(95)00233-3.
- 225 Arai, S., and Akizawa, N., 2014, Precipitation and dissolution of chromite by
226 hydrothermal solutions in the Oman ophiolite: New behavior of Cr and chromite:
227 *American Mineralogist*, v. 99, p. 28–34, doi:10.2138/am.2014.4473.

- 228 Bach, W., and Klein, F., 2009, The petrology of seafloor rodingites: Insights from
229 geochemical reaction path modeling: *Lithos*, v. 112, p. 103–117,
230 doi:10.1016/j.lithos.2008.10.022.
- 231 Benoit, M., Polvé, M., and Ceuleneer, G., 1996, Trace element and isotopic
232 characterization of mafic cumulates in a fossil mantle diapir (Oman ophiolite):
233 *Chemical Geology*, v. 134, p. 199–214, doi:10.1016/S0009-2541(96)00087-3.
- 234 Benoit, M., Ceuleneer, G., and Polvé, M., 1999, The remelting of hydrothermally altered
235 peridotite at mid-ocean ridges by intruding mantle diapirs: *Nature*, v. 402, p. 514–
236 518, doi:10.1038/990073.
- 237 Berndt, J., Koepke, J., and Holtz, F., 2005, An experimental investigation of the influence
238 of water and oxygen fugacity on differentiation of MORB at 200 MPa: *Journal of*
239 *Petrology*, v. 46, p. 135–167, doi:10.1093/petrology/egh066.
- 240 Borisova, A.Y., et al., 2012, A new view on the petrogenesis of the Oman ophiolite
241 chromitites from microanalyses of chromite-hosted inclusions: *Journal of Petrology*,
242 v. 53, p. 2411–2440, doi:10.1093/petrology/egs054.
- 243 Bosch, D., Jamais, M., Boudier, F., Nicolas, A., Dautria, J.M., and Agrinier, P., 2004,
244 Deep and high-temperature hydrothermal circulation in the Oman ophiolite—
245 Petrological and isotopic evidence: *Journal of Petrology*, v. 45, p. 1181–1208,
246 doi:10.1093/petrology/egh010.
- 247 Bowen, N.L., and Tuttle, O.F., 1949, The system MgO-SiO₂-H₂O: *Geological Society of*
248 *America Bulletin*, v. 60, p. 439–460, doi:10.1130/0016-
249 7606(1949)60[439:TSM]2.0.CO;2.

- 250 Ceuleneer, G., Nicolas, A., and Boudier, F., 1988, Mantle flow patterns at an oceanic
251 spreading centre: The Oman peridotites record: *Tectonophysics*, v. 151, p. 1–26,
252 doi:10.1016/0040-1951(88)90238-7.
- 253 Ceuleneer, G., Monnereau, M., and Amri, I., 1996, Thermal structure of a fossil mantle
254 diapir inferred from the distribution of mafic cumulates: *Nature*, v. 379, p. 149–153,
255 doi:10.1038/379149a0.
- 256 Coogan, L.A., 2003, Contaminating the lower crust in the Oman ophiolite: *Geology*,
257 v. 31, p. 1065–1068, doi:10.1130/G20129.1.
- 258 Dick, H.J.B., 1977, Evidence of partial melting in the Josephine Peridotite, *in* Dick,
259 H.J.B., ed., *Magma Genesis 1977: Proceedings of the American Geophysical Union*
260 *Chapman Conference on Partial Melting in the Earth's Upper Mantle: State of*
261 *Oregon Department of Geology and Mineral Industries*, p. 59–62.
- 262 Dygert, N., and Liang, Y., 2015, Temperatures and cooling rates recorded in REE in
263 coexisting pyroxenes in ophiolitic and abyssal peridotites: *Earth and Planetary*
264 *Science Letters*, v. 420, p. 151–161, doi:10.1016/j.epsl.2015.02.042.
- 265 Elthon, D., 1979, High magnesia liquids as the parental magma for ocean floor basalts:
266 *Nature*, v. 278, p. 514–518, doi:10.1038/278514a0.
- 267 Gillis, K.M., and Meyer, P.S., 2001, Metasomatism of oceanic gabbros by late stage
268 melts and hydrothermal fluids: Evidence from the rare earth element composition of
269 amphiboles: *Geochemistry, Geophysics, Geosystems*, v. 2, 1012,
270 doi:10.1029/2000GC000087.
- 271 Gillis, K.M., et al., 2014, Primitive layered gabbros from fast-spreading lower oceanic
272 crust: *Nature*, v. 505, p. 204–207, doi:10.1038/nature12778.

- 273 Greenbaum, D., 1972, Magmatic processes at ocean ridges: Evidence from Troodos
274 massif, Cyprus: *Nature*, v. 238, p. 18–21, doi:10.1038/physci238018a0.
- 275 Gregory, R.T., and Taylor, H.P., 1981, An oxygen isotope profile in a section of
276 Cretaceous oceanic crust, Samail Ophiolite, Oman: Evidence for $\delta^{18}\text{O}$ buffering of
277 the oceans by deep (>5 km) seawater-hydrothermal circulation at mid-ocean ridges:
278 *Journal of Geophysical Research*, v. 86, p. 2737–2755,
279 doi:10.1029/JB086iB04p02737.
- 280 Kelemen, P.B., Shimizu, N., and Salters, V.J., 1995, Extraction of mid-ocean-ridge
281 basalt from the upwelling mantle by focused flow of melt in dunite channels: *Nature*,
282 v. 375, p. 747–753, doi:10.1038/375747a0.
- 283 Koepke, J., Berndt, J., Horn, I., Fahle, J., and Wolff, P.E., 2014, Partial melting of
284 oceanic gabbro triggered by migrating water-rich fluids: A prime example from
285 the Oman Ophiolite, *in* Rollinson, H.R., et al., eds., *Tectonic evolution of the*
286 *Oman Mountains: Geological Society of London Special Publication 392*, p. 195–
287 212, doi:10.1144/SP392.10.
- 288 Korenaga, J., and Kelemen, P.B., 1997, Origin of gabbro sills in the Moho transition zone
289 of the Oman ophiolite: Implications for magma transport in the oceanic lower crust:
290 *Journal of Geophysical Research*, v. 102, p. 27,729–27,749, doi:10.1029/97JB02604.
- 291 MacLeod, C.J., Lissenberg, C.J., and Bibby, L.E., 2013, “Moist MORB” axial
292 magmatism in the Oman ophiolite: The evidence against a mid-ocean ridge origin:
293 *Geology*, v. 41, p. 459–462, doi:10.1130/G33904.1.


- 294 Moores, E.M., and Vine, F.J., 1971, The Troodos massif, Cyprus and other ophiolites as
295 oceanic crust—Evaluation and implications: Royal Society of London Philosophical
296 Transactions, ser. A, v. 268, p. 443–467, doi:10.1098/rsta.1971.0006.
- 297 Newton, R.C., and Manning, C.E., 2007, Solubility of grossular, $\text{Ca}_3\text{Al}_2\text{Si}_3\text{O}_{12}$, in H_2O -
298 NaCl solutions at 800° C and 10kbar, and the stability of garnet in the system
299 CaSiO_3 - Al_2O_3 - H_2O -NaCl: *Geochimica et Cosmochimica Acta*, v. 71, p. 5191–5202,
300 doi:10.1016/j.gca.2007.08.021.
- 301 Pearce, J.A., Alabaster, T., Shelton, A.W., and Searle, M.P., 1981, The Oman ophiolite as
302 a Cretaceous arc-basin complex: Evidence and implications: Royal Society of
303 London Philosophical Transactions, ser. A, v. 300, p. 299–317,
304 doi:10.1098/rsta.1981.0066.
- 305 Python, M., and Ceuleneer, G., 2003, Nature and distribution of dykes and related melt
306 migration structures in the mantle section of the Oman ophiolite: *Geochemistry,*
307 *Geophysics, Geosystems*, v. 4, 8612, doi:10.1029/2002GC000354.
- 308 Python, M., Ceuleneer, G., Ishida, Y., Barrat, J.A., and Arai, S., 2007, Oman diopsidites:
309 A new lithology diagnostic of very high temperature hydrothermal circulation in
310 mantle peridotite below oceanic spreading centres: *Earth and Planetary Science*
311 *Letters*, v. 255, p. 289–305, doi:10.1016/j.epsl.2006.12.030.
- 312 Python, M., Yoshikawa, M., Shibata, T., and Arai, S.,
313 2011, Diopsidites and rodingites: Serpentinisation and Ca-metasomatism in the
314 Oman Ophiolite mantle, *in* Srivastava, R.K., ed., *Dyke swarms: Keys for*
315 *geodynamic interpretation*: Berlin, Springer-Verlag,
316 doi:10.1007/978-3-642-12496-9_23.

- 317 Rabinowicz, M., Ceuleneer, G., and Nicolas, A., 1987, Melt segregation and flow in
318 mantle diapirs below spreading centers: evidence from the Oman ophiolite: Journal
319 of Geophysical Research, v. 92, p. 3475–3486, doi:10.1029/JB092iB05p03475.
- 320 VanTongeren, J.A., Kelemen, P.B., and Hanghøj, K., 2008, Cooling rates in the lower
321 crust of the Oman ophiolite: Ca in olivine, revisited: Earth and Planetary Science
322 Letters, v. 267, p. 69–82, doi:10.1016/j.epsl.2007.11.034.
- 323 Wang, C., Liang, Y., Dygert, N., and Xu, W., 2016, Formation of orthopyroxenite by
324 reaction between peridotite and hydrous basaltic melt: An experimental study:
325 Contributions to Mineralogy and Petrology, v. 171, 77, doi:10.1007/s00410-016-
326 1287-z.
- 327 Yamasaki, T., Maeda, J., and Mizuta, T., 2006, Geochemical evidence in clinopyroxenes
328 from gabbroic sequence for two distinct magmatisms in the Oman ophiolite: Earth
329 and Planetary Science Letters, v. 251, p. 52–65, doi:10.1016/j.epsl.2006.08.027.

330 **FIGURE CAPTIONS**

331 Figure 1. A: Location of the Oman ophiolite. B: Geological map of the southeast massifs
332 of the Oman ophiolite showing the Maqsad paleo-ridge segment (red outline) and the
333 inferred position of the paleo-spreading axis (red dotted line) (Python and Ceuleneer,
334 2003). C: Enlargement of the Maqsad diapir area; orange lines indicate the positions of
335 our cross sections.

336

337 Figure 2. Synthetic lithological log showing the vertical distribution of the mineral
338 assemblages along the dunitic transition zone (DTZ) in the vicinity of the Maqsad diapir,
339 Oman. Pl—plagioclase; Ol—olivine. 

340

341 Figure 3. Photomicrographs showing the texture of the various minerals constituting the
342 dunitic transition zone dunites and phases enclosed as inclusions in chromite grains. A:
343 500 μm clinopyroxene (tiny diopside) underlying olivine grains. B: Interstitial grossular
344 garnet (sporadically associated with hydrogrossular and andradite; see the Data
345 Repository; see footnote 1). C: Interstitial pargasite (frequently associated with
346 magnesiohornblendes and rare magnesio-hastingsites). D: Oikocrystic orthopyroxene in
347 dunite showing lobate contacts with olivine. E, F: Inclusions of garnet, clinopyroxene,
348 hybrid diopside, orthopyroxene, and amphibole in chromite.

349

350 Figure 4. Major element compositions of clinopyroxene (cpx), amphibole (amph), and
351 orthopyroxene (opx) observed interstitially in dunite and in inclusion in chromites. A:
352 Al_2O_3 and TiO_2 versus Mg# in clinopyroxene. B: TiO_2 versus Al_2O_3 and $(\text{Na}^+\text{K})_{\text{A}}$ versus
353 Al_{IV} in amphiboles. C: TiO_2 versus Mg# in orthopyroxene.

354

355

356 ¹GSA Data Repository item 2017xxx

357 , is available online at

358 <http://www.geosociety.org/datarepository/2017/> or on request from

359 editing@geosociety.org.